Experimental investigation of the low temperature oil-on-water cooling and lubrication in turning the hardened AISI D2 steel

Jihui Zhang (823870037@qq.com)
Northwest Minzu University
Linhu Tang
Furong Ma
Yanjun Hu
Baodong Li
Yongji Sun

Research Article

Keywords: Hard turning, LTOoW, Cutting force, Surface roughness, Cutting temperature, Tool wear

Posted Date: March 11th, 2022

DOI: https://doi.org/10.21203/rs.3.rs-1425393/v1

Version of Record: A version of this preprint was published at The International Journal of Advanced Manufacturing Technology on January 4th, 2023. See the published version at https://doi.org/10.1007/s00170-022-10692-4.

Abstract

In this paper, the influence of the cutting speed, feed, and the depth of cut on the cutting force, surface roughness, cutting temperature, and tool wear were experimentally investigated under the low temperature oil-on-water (LTOoW) cooling and lubrication condition in turning the hardened tool steel AISI D2 (60±1HRC) with the PCBN cutting tool. The results showed that the three-component cutting forces is $F_Y > F_Z > F_X$ and the cutting speed has more significant effect on the ratio of F_Y/F_Z at the range of 55-495 m/min cutting speed, 0.05-0.25 mm feed, and 0.05-0.25 mm depth of cut. The influence of the cutting speed on the cutting temperature is slightly more visible compared to the feed and depth of cut. In this experiment, a satisfactory surface roughness value of 0.54 μm can be obtained, gaining the effect of the turning instead of the grinding. The flank wear values of the PCBN tool are 142 μm and 148 μm respectively at the cutting speeds of 55 and 140 m/min; however, the flank wear value abruptly increases to 668 μm at a 495 m/min, which has a very serious impact on the tool life. The abrasive wear is considered to be a predominant wear mechanism on the flank wear of PCBN tool. The rake face is dominated by crater wear due to the high temperature, high pressure, high stress and high friction at the chip-tool interface.

Introduction

In recent years, with the increasing demands on the mechanical and other properties of the parts, some difficult-to-machine materials with hardness as high as 50–70 HRC, such as the hardened tool steel AISI D2, have emerged. It is widely used in industrial fields such as bearings and molds due to its mechanical strength, fatigue resistance and wear resistance.

It is accompanied by waste liquid pollution, low processing efficiency, and difficult to guarantee product quality as machining these materials in traditional processing technology. [1] In the past 30 years, many researchers have been focusing on the dry hard cutting technology in order to avoid its substantial disadvantages. Although dry hard cutting technology has the advantages of high processing accuracy, high production efficiency, and less environmental pollution, [2] it also has disadvantages such as the high cutting temperature, large cutting force, and short tool life. [3] Nevertheless, these green machining technologies, such as low temperature cold air (LTCA), minimal quantity lubrication (MQL), and oil on water (OoW) have always been focused by various researchers in recent years [4] because they have been considered to be the replacement for dry machining.

The LTCA cutting technology is a cooling and lubrication technique that sprays low-temperature compressed air into the cutting zone to reduce the temperature of the cutting zone. In 2010, Sun et al. [5] have conducted an experimental study on the LTCA in turning of titanium alloys and confirmed that it has a longer tool life and higher machined surface quality than the dry cutting. Furthermore, Su et al. [6] also have come to the conclusion that the LTCA cutting can significantly prolong the tool life and improve the quality of the machined surface. Next year, Boswell et al. [7] from Australia have conducted cutting tests by using the LTCA + minimal quantity lubrication (MQL) technology. According to the findings of the

research, the LTCA + vegetable oil MQL technology is the most promising cooling and lubrication technology. The machining performance of Ti-6Al-4V titanium alloy under the condition of LTCA has been studied by Liu et al. in 2013. [8] They have pointed out that, compared with dry cutting, LTCA can significantly reduce the cutting temperature, prolong tool life, as well as obtain the best machined surface. Subsequently, Jozic et al. [9] have optimized the cutting parameters in milling 42CrMo4 under the conditions of the cutting fluid, LTCA, and dry cutting by using the orthogonal experiment in 2015. It has been discovered by Kopac et al. [10] that the residual compressive stress conducive to improving the machined surface quality can be obtained after the low temperature machining. Moreover, Arruda et al. [11] have considered a significantly longer tool life in cutting API 5L X70 steel under LTCA condition.

The MQL cutting technology is also a cooling and lubrication technique that sprays the minimum quantity of lubricant oil mist mixed up with compressed air into the cutting zone to decrease temperature and friction in chip-tool-workpiece interface, reduc tool wear, and improve the quality of the machined surface. Anthony-Xavior et al. [12] have investigated the influence of the coconut oil, emulsion, and oily cutting fluid on the surface roughness and tool wear in turning AISI 304 steel. It has a great impact on improving the surface roughness and extending the tool life. Besides, Saini et al. [13] have experimentally investigated the influence of variables such as cutting speed, feed, and depth of cut, etc. on the cutting force and tool tip temperature in turning AISI 4340 steel at different environmental conditions of dry and MQL cutting. The results obtained in this paper showed that the main cutting force is largest among the three-component cutting forces, and that MQL cutting has an excellent lubricating effect when compared with dry cutting. In 2017, Pervaiz et al. [14] have experimentally evaluated such important indicators as the surface roughness, cutting force, tool life, and other important indicators focused by the machinists in turning titanium alloy Ti-6Al-4V at the condition of low temperature MQL. Masoudi et al. [15] have considered that the MQL system significantly increases the cutting efficiency after researched the influences of different parameters on the tool wear, cutting force, and surface roughness in machining AISI 1045 steel. Currently, Makhesana et al. [16] have further investigated the surface roughness, chip-tool interface temperature, and tool life in turning AISI 4140 steel with coated carbide tools under the cooling and lubrication conditions of vegetable oil-based MQL (VMQL) and minimum quantity solid lubricant (MQSL). The results showed that VMQL and MQSL have significant advantages compared to dry cutting.

The OoW droplets cutting technology refers to the processing technology that sprays a small amount of compressed and atomized vegetable oil and water into the cutting zone to reduce the cutting temperature and lubricate the chip-tool-workepiece interfaces. In 2015, Lin et al. [17] have analyzed and compared the tool wear at two cooling and lubrication conditions of the OoW droplets and LTCA in turning of titanium alloy Ti-6Al-4V. They have considered that it can obtain lower surface roughness values and lower tool wear by using the OoW cooling lubrication technology. Then, Wang et al. [18] have studied the tool wear mechanism in turning compacted graphite cast iron at different OoW droplets cooling conditions in 2017. The cooling and lubrication technology has been shown to prolong the life of the cutting tool. Moreover, the influence law and internal mechanism of the nozzle position and diameter on surface roughness and tool wear have been investigated by Yao et al. [19] under the condition of OoW droplets cooling and lubrication.

According to a large number of literatures, cooling and lubricating techniques such as the LTCA, MQL, and OoW can all achieve satisfactory results, and each has its own advantages. Such difficult-to-machine materials as the hardened AISI D2 tool steel necessitates the use of an innovative cooling and lubrication technology to minimize the cutting temperature at the cutting zone. In this paper, an innovative low temperature oil on water (LTOoW) mist cooling and lubrication technology was proposed by combining the three cooling and lubrication technologies of MQL + OoW+(LTCA). And the influence law and mechanism of the cutting speed, feed, and depth of cut on the cutting force, surface roughness, cutting temperature, as well as tool wear, will be experimentally investigated by using the PCBN cutting tool in turning the hardened tool steel AISI D2 (60 ± 1HRC).

Mechanism Of The Ltoow Cooling And Lubrication Technology

The low temperature oil on water (LTOoW) mist technology is a cooling and lubrication technology that the low temperature compressed air (-20–-30 ℃) mixed with the minimum vegetable oil and water does converge at the atomization nozzle to form a low temperature oil on water mist jet.

As shown in Fig. 1, the oil in the low temperature medium is attached to the surface of the water drops and is sprayed into the high temperature cutting zone at the chip-tool-workpiece interfaces by the nozzle at high speed, high pressure, and high kinetic energy to form a lubricating film. It plays the cooling and lubrication of the chip-tool-workpiece interfaces, thus reducing the friction at the chip-tool-workpiece interfaces and cutting force.

The low temperature water droplets sprayed into the high-temperature cutting zone are instantly vaporized in the high temperature environment at the chip-tool- workpiece interfaces, taking away a large amount of cutting heat and reducing the cutting temperature. The formed boundary lubrication film not only reduces the cutting force, but also reduces the tool wear, and even improves the machined surface quality. On the one hand, the high pressure, high speed, and low temperature airflow in the cutting zone has the cooling effect due to forced convection and an increase in temperature difference. On the other hand, it is conducive to the chip removal, reducing the contact area and friction at the tool-chip, thereby reducing the tool wear of the rake face.

These combined effects avoid the loss of lubricating effect of the lubrication film at the chip-tool-workepiece interfaces due to too high temperature in the cutting zone, which has obvious advantages compared to the normal temperature MQL technology.

Experimental Procedures

2.1 Workpiece material and heat treatment

The workpiece material was the hardened tool steel AISI D2 (Cr12MoV, China), and the chemical composition and content are displayed in Table 1. The specimen is 128 mm in diameter, 210 mm in length, 6 mm in trough width and 80 mm in ring width, as shown in Fig. 2 (a). After heat treatment at

1040°C and low temperature tempering, the hard layer on the workpiece surface was removed to obtain a workpiece with a hardness of 60 ± 1 HRC. The quenching hardness of the specimen was determined by a digital Rockwell hardness tester (type: HRS-150), as shown in Fig. 2(b).

Table 1
Chemical composition and content of the AISI D2 tool steel (wt.%)

C	Cr	Mo	Mn	Si	P	S	V
1.55	11.25	0.45	0. 35	0.35	0.025	0.025	0.20

2.2 Tool composition, performance, and geometric parameters

According to the literature [20], a polycrystalline cubic boron nitride (PCBN) tools with a CBN content of 50% were selected. The composition and properties of CBN are shown in Table 2. The geometric angle design with negative rake angle and chamfer was selected to improve the strength of the somewhat brittle PCBN composite tool. The effective geometric parameters are shown in Table 3. The PCBN composite tool used in this experiment is shown in Fig. 3.

Tab. 2 Composition and performance of the PCBN tool

Type (America)	Percent by volume /%	Grain size/μm	Dinder	Density/g/mm^3
GE2100	50	2	TiN	3.5

Tab. 3 The effective geometry parameters of PCBN tool

κ_r /°	κ_r'/°	γ_0/°	α/°	γ_0'/°	λ_s/°	r_ε/mm	β/°	b/mm
75°	15°	-10°	7°	5°	-4°	0.8	-15°	0.1

2.3 Turning experiment system

Figure 4 shows the schematic diagram of the turning experiment system, which consists of a turning testing- measuring system, a LTOoW cooling and lubrication system, and other measuring instruments such as a surface roughness tester, etc..

The turning experiment system consists of a common lathe (type: CA6140), a Kistler dynamometer (type: 9257C), and a high speed infrared temperature measurement intelligent acquisition system (type: DM63-II), as shown in Fig. 5. The average values of the cutting forces data collected in the steady-state cutting stage are taken as the three-component cutting forces, and the obtained highest temperature during the period is the cutting temperature.

2.4 LTOoW mist cooling and lubrication system

The LTOoW mist cooling and lubrication system consists of the air compressor, air storage tank, low temperature compound spray cooling equipment (type: AR-800-OoW-55), as well as an atomizing nozzle with a diameter of 0.8 mm, as shown in Fig. 6(a) and (b). The compressed air from the screw air compressor (type: LDB-10A/8) is stored in the air storage tank in order to obtain a stable air source and enters the low temperature composite cooling equipment; and then the low temperature airflow is generated after heat exchange.

The low temperature airflow, as well as the low temperature gas, oil and water mixture pressed from the oil and water tanks, is converged at the atomizing nozzle and sprayed a LTOoW mist at a low temperature of -30 °C after repeated adjusting the low-temperature cold air control system. Fig. 6(c) presents the jet temperature field at the nozzle collected by the thermal imager after repeated debugging. The vegetable oil-based micro-cutting oil (type: MIRCOLUBE 2000-30) was selected to be the cooling and lubricant. The detailed parameters of the cooling and lubrication system used in this experiment are shown in Tab. 4.

Table 4
Parameters of the LTOoW cooling and lubrication system

Open valve	Parameter name	parameter value
Cold air	Cold air temperature/℃	-30 ℃
	Rate of flow/L/min	120
	Pressure/MPa	0.8
Oil mist	Oil pressure/MPa	0.6
	Rate of flow/mL/h	20
Water	Water pressure/MPa	0.6
	Oil to water flow ratio	1:100

2.5 Measurement of surface roughness

As shown in Fig. 7, the surface roughness values were measured by utilizing the SJ-210 portable surface roughness tester. It was measured five times along the circumference of each turning ring surface, and then the average value was taken as the final surface roughness.

2.6 Measurement and analysis of the tool wear

The rake face and flank wear and morphology of the PCBN cutting tools (Fig. 8) were measured by a Zeiss ultra-depth microscope (type: Smartzoom5) as shown in Fig. 9(a). And the average value of the three measurement readings was taken as the evaluation value. The analysis and observation of the micro-morphology and tool wear mechanism were completed by a thermal field electron microscope (type: INSPECT F50, SEM) equipped with an energy dispersive X-ray spectrometer (EDS) detector, as

shown in Fig. 9(b). In this part of the experiment, the cutting parameters of the 55, 140, 249, 395, and 495-m/min cutting speed, a fixed 0.15-mm/r feed, 0.15-mm depth of cut, and 215-m spiral cutting length were chosen to investigate the tool wear.

Results And Discussion

3.1 Cutting force

Fig.10 describes the influent of the cutting speed on the three-component cutting forces in range from 55 to 495-m/min cutting speed at the fixed 0.15-mm/r feed and 0.15-mm depth of cut. Fig. 10(a) shows the variation of the three-component cutting forces with increments of the cutting time in a case of 140-m/min cutting speed in turning hardened tool steel AISI D2 (60±1HRC). As shown in Fig. 10(b), the three-component cutting forces are F_Y>F_Z>F_X in the range of 55-495 m/min, which is a remarkable characteristic of the hard cutting. This is similar to the results of the literature [21]. It can be seen in Fig. 10(b) that when the cutting speed gradually increases, the feed force and the main cutting force change relatively flat, while the radial cutting force gradually increases. Especially in the case of 495-m/min cutting speed, it increases sharply by 103%. Considering the influence of the cutting force on the tool life and machining accuracy, it is more economical to machine in the range of 55-395 m/min, instead of 495 m/min.

So what is the reason that the radial cutting force increases sharply at 495 m/min, while the other two-component cutting forces change less? It should be that the adhesion effect of the chips softened by high temperature at the cutting zone increases the frictional force at the chip-tool interface, resulting in an abrupt increase of the radial cutting force, which is similar to the results of the literature' results [2].

Figure 11 describes the influent of the feed on the three-component cutting forces in range of 0.05-0.25-mm/r feed at the fixed 249-m/min cutting speed and 0.15-mm depth of cut. Figure 11(a) shows the variation of the three-component cutting forces with increments of the cutting time in a case of 0.10-mm/r feed, 249-m/min cutting speed, and 0.15-mm depth of cut. As shown in Fig. 11(b), the three-component cutting forces are also F_Y>F_Z>F_X in the range of 0.05-0.25-mm/r feed. Moreover, the feed has greater influence on the radial cutting force compared to cutting speed, which increases rapidly and linearly. While the main cutting force gradually increases and reaches a peak of 106 N in a case of 0.20-mm/r feed, and then gradually decreases.

Fig.12 illustrates the influent of the depth of cut on the three-component cutting forces in range of 0.05-0.25-mm depth of cut at the fixed 249-m/min cutting speed and 0.15-mm/r feed. Fig. 12(a) shows the variation of the three-component cutting force with increments of the cutting time in a case of 0.10-mm depth, 249-m/min cutting speed, and 0.15-mm feed. As shown in Fig. 12(b), the variation law and characteristics of the three-component cutting force are very similar to the influence of the cutting speed in the range of 0.05-0.25-mm depth of cut, which is not be repeated here.

3.2 Surface roughness

Figs. 13, 14, and 15 describe the influence of the cutting speed, feed, and depth of cut on the surface roughness. The surface roughness value firstly gradually decreases with increments of the cutting speed, as observed in Fig. 14. The minimum value of 0.90 μm is obtained in a case of 249 m/min; it slightly increases to 1.02 μm at 395 m/min, and then rapidly increases to 2.32 μm at 495 m/min. As observed in Fig. 19, it is the severe flank wear that results in deteriorating the machined surface quality. It can be clearly observed in tab. 5 that the more serious serrated nose wear at the nose part of the PCBN inserts may explain why the roughness in cases of 55 and 495 m/min begins to deteriorate. And the sharply flattened nose radius induced by tool wear should contribute to the reduction of surface roughness at 249 and 395 m/min, as presented in this table.

It can be clearly visible in Fig. 14 that with increments of the feed, the surface roughness value gradually increases, which is consistent with the conventional metal cutting theory. The surface roughness values of 0.54 and 0.56μm can be obtained respectively in the feeds of 0.05 and 0.10 mm/r, which gains the effect of the turning instead of grinding.

As observed in Fig. 15, the effect of depth of cut on the surface roughness is very little, but it is very interesting that the surface roughness value reaches the minimum value in a case of 0.15-mm depth of cut.

Combining with Fig. 10, 13, and 19, it can be seen that not only the cutting force is smaller, the surface roughness value is the smallest, but also the tool life is longer as selecting the cutting parameter of 249-m/min cutting speed, 0.15-mm/r feed, and 0.15-mm depth of cut, which is a set of relatively satisfactory cutting parameters.

3.3 Cutting temperature

Here, the cutting temperature known as one of the crucial issues was investigated because it highly influences the tool life and machined workpiece surface quality.

Figs. 16, 17, and 18 present the temperature field of the cutting zone collected in real time by the thermal imager and the variation law of the maximum temperature with increments of the cutting speed, feed, and depth of cut, respectively. As observed in Fig. 16(b), that the cutting temperature gradually increases with increments of the cutting speed, and that it varies in the range of 230-340 °C. And it remains basically unchanged between 300°C and 330 °C with increments of the feed, as seen in Fig. 17(b). It also tends to increase with the increments of the depth of cut, and the maximum temperature in the cutting zone varies from 260 to 333 °C, as shown in Fig. 18(b). Although the collected cutting temperature may be lower than that in cutting zone due to the lag in the response time of the thermal imager and the rapid heat dissipation of the chip temperature, its variation law is real and credible.

The experimental results show that the maximum cutting temperature does reach the peak of 340°C at the LTOoW mist cooling and lubrication condition, far being lower than the peak cutting temperature of 770°C described in dry cutting in the literature [3], which indicates that the generated high heat is absorbed by the water mist during evaporation.

3.4 Tool wear

3.4.1 Wear law of the PCBN cutting tool

Since the influence of the cutting speed on the tool wear is the most important key one among three cutting variables, and the mechanism is also the most complicated, [22] in this experiment, the influence and mechanism of the cutting speed on the tool wear were investigated at cutting speeds of 55, 140, 249, 395 and 495 m/min at fixed 0.15-mm/r feed, 0.15-mm depth of cut, and 215-mm spiral cutting length. The rake face and flank wear of the PCBN tool at the five cutting speeds is shown in Table 5.

As shown in Fig. 19, the flank wear V_{Bmax} of the PCBN tool basically does not change and is 142 μm and 148 μm at the cutting speeds of 55 and 140 m/min, respectively, which is in good agreement with the allowable wear criteria of $[V_B]$ = 0.3 mm [23]. When the cutting speed reaches 249 m/min, the flank wear V_{Bmax} suddenly increases, and its value runs up to 319 μm; and then it slightly increases to 340 μm at a cutting speed of 495 m/min. It is obvious that the flank wear meets the allowable wear criteria $[V_B]$ = 0.4 mm [23] as the spiral cutting length reaches 215 m at the two cutting speeds. When the cutting speed reaches 495 m/min, the flank wear begins to deterioarate and drastically increases to 668 μm, with an increase of about 109%, which is in good agreement with the variation of radial cutting force as shown in Fig. 10. Obviously, if only the tool life factor is considered, the cutting speeds of 55 and 140 m/min are two more appropriate cutting speeds in turning hardened tool steel AISI D2 (60 ± 1 HRC). However, the cutting speed of 495 m/min has a deteriorative influence on the flank wear of the PCBN tool and is not suitable for cutting, as also confirmed in Table 5 and Fig. 20(e).

3.4.2 Tool wear mechanism

(1) Flank wear

The wear region of the flank and rake face was analyzed by scanning electron microscope in order to further study the flank wear mechanism.

It can be noticed in Figs. 20(a)-(e) and Table 5 that when the spiral cutting length runs up to 215 m, deep grooves occur on the flank, which indicates that the abrasive wear on the flank is the dominant wear mechanism. The binder is more prone to chemical, dissolution and diffusion wear than the BN due to high temperature, high load and high stress, resulting in the falling off of loose CBN particles. The grooves on the flank should be caused by the rolling and sliding of these loose CBN particles or hard carbon particles at the tool-chip interface.

It must be noted that, as observed in Table 5 and Figs. 19 and 20, the chipping and delamination wear generate at the cutting speed of 495 m/min. Figure 19 can explain the internal mechanism inducing this phenomenon. The figure shows that the radial cutting force suddenly increases to 420 N at a 495 m/min, which increases the friction at tool-workepiece interface, resulting in more serious abrading and tearing on the flank, which leads to more serious chipping and delamination wear on the flank. Moreover, the

generation of higher temperature at a 495 m/min shown in Fig. 16 should be responsible for faster growth of tool wear, too.

(2) Rake face wear

It can be observed in Figs. 20(a)-(e) that the crater wear is the most typical wear form on the rake face of the PCBN tool. The crater region justly located in the high temperature and the larger mechanical load zone, which will result in high normal stress and high shear stress caused by the tool-chip friction effect. As shown in Fig. 16, the temperature field obtained by the infrared thermal imager shows that the cutting temperature reaches a peak of approximate 340°C as the cutting speed reaches 495 m/min. In fact, the temperature at the cutting edge must be far higher than this. Such high temperature must leads to adhesive wear, delamination wear, and diffusion wear, and then accelerates the crater wear and eventually induces serious damage to the rake face.

It can be seen in Fig. 20 that the adhesive wear and diffusion wear do occur at the rear of the crater region, and the cutting temperature, friction force, pressure and compressive stress in this region are lower than those in the crater region. However, the friction at the tool-chip interface results in abrading and tearing effects, which must induce two cases: first, the chip material may remain in the crater; secondly, the material on the rake surface should be adhered away by the high-temperature chip to form adhesive wear, as shown in Figs. 20(a)-(e).

According to the literature [24], the calculation formula of the tool-chip interface friction coefficient is:

$$\mu = \frac{F_{\mathrm{X}} \cos \gamma_0 - F_Z \sin \gamma_0}{F_{\mathrm{X}} \cos \lambda_s \sin \gamma_0 + F_{\mathrm{Y}} \sin \lambda_s + F_Z \cos \lambda_s \cos \gamma_0}$$

1

Taking the main, radial, and feed forces shown in Fig. 10 and the effective tool geometry parameters in Table 3 into formula (1), it can be obtained that the friction coefficient at a 495 m/min abruptly increases to 0.65. It can be observed that the friction force loaded at the crater region on the rake face of the PCBN tool becomes very large. As a result, a large plastic strain within the rake sub-surface leads to the thermal micro-crack initiation in this region, resulting in a large piece of delamination wear on the rake face of the tool as shown in Fig. 20(e), which is similar to the earlier literature [25].

Furthermore, as clearly shown in Figs. 20(a)-(b), workpiece material can be transferred to the tool surface. The deposition of workpiece material in crater is much more at lower cutting speed when compared to other higher cutting speeds. This may be the reason that the back of the softened chip has sufficient time to adhered with the rake face due to the relatively lower speed of chips flying away from the rake face as turning at the lower cutting speeds of 55 and 140 m/min, which results in more softened chips staying in the crater; while the crater has very little adhered material at higher cutting speeds of 249, 395, and 495 m/min.

Figure 21 presents the EDS analysis of adhered material in crater on the rake face at a 395 m/min. It can be seen in the figure that except for the chemical elements (B, N, Ti) of the PCBN tool and the main chemical elements (Fe, C, Cr, Mo, V, Si) of workpiece material, the oxygen element was also detected. It indicates that these adhered materials should be metal and non-metal oxide.

Conclusions

The cutting force, surface roughness, cutting temperature, tool wear were experimentally investigated and analyzed in turning hardened tool steel AISI D2 (60 ± 1 HRC) with the PCBN tool at the condition of the LTOoW mist cooling and lubrication. The conclusions are as follows:

(1) The three-component cutting force becomes $F_Y > F_Z > F_X$, which should be a significant characteristic of the hard cutting; while the influent of the cutting speed on the ratio of F_Y/F_Z is more significant compared with the other two parameters.

(2) The maximum cutting temperature does reach the peak of 340°C at the LTOoW mist cooling and lubrication condition, far being lower than the peak cutting temperature in dry cutting.

(3) The surface roughness value reaches 0.54 μm in a case of v = 249 m/min; f = 0.05 mm/r; a_c=0.15 mm, which gains the effect of the turning instead of the grinding. The influence of cutting depth on surface roughness becomes less, and it varies in the very small range of 0.87 to 1.029 μm.

(4) The flank wear values of the PCBN tool basically does not change and are 142 μm and 148 μm respectively at the cutting speeds of 55 and 140 m/min; however, it abruptly increases to 668 μm at a 495 m/min, which has a very serious impact on the tool life.

(5) The rolling and sliding of the loose CBN or hard carbon particles at the tool-chip interface is the predominant reason inducing abrasive wear on the PCBN flank. Meanwhile, a large plastic strain within the rake sub-surface leads to the thermal micro-crack initiation in this region, resulting in a large piece of delamination wear on the rake face of the tool. The rake face wear of the PCBN is dominated by crater wear due to the high temperature, high pressure, high stress, and high friction at the chip-tool interface.

Abbreviations

v Cutting speed (meter per minute)

f Feed (millimeter per revolution)

a_c Depth of cut (millimeter)

F_X Feed cutting force (N)

F_Y Radial cutting force (N)

F_z Main cutting force (N)

K_r Major cutting-edge angle (degrees)

κ_r' End-cutting edge angle (degrees)

γ_0 Rake angle (degrees)

α Clearance angle (degrees)

γ_0' Side clearance angle (degrees)

λ_s Inclination angle (degrees)

r_ε Nose radius (millimeter)

b Chamfer width ((millimeter)

β Chamfer angle (degrees)

L Spiral cutting length

LTOoW Low temperature oil-on-water

Declarations

Acknowledgments The authors would like to thank the Provincial Key Laboratory for Green Cutting Technology and Application of Gansu Province, and the Key Laboratory for Utility of Environment-Friendly Composite Materials and Biomass in University of Gansu Province.

Authors' contributions All authors contributed to the material preparation, data collection and experimental study. All authors commented on previous versions of the manuscript. All authors read and approved the final manuscript.

Funding This work was supported by National Natural Science Foundation of China (Grant No. 51965031), and the Natural Science Foundation of Gansu Province in China (Grant No. 20JR5RA376).

Availability of data and material Not applicable.

Code availability Not applicable.

Ethics approval I certify that the manuscript has never been published or submitted for publication elsewhere.

Consent to participate Not applicable.

Consent for publication All authors agree to publish.

Conflicts of interest I, Jihui Zhang, corresponding author of the paper, certify that we have no potential conflict of interest for the presented article.

References

1. Lawal SA, Choudhury IA, Nukman Y (2012) Application of vegetableoil-based metalworking fluids in machining ferrous metals—A review. Int J Mach Tools Manuf 252:1–12
2. Tang L, Gao C, Huang J, Shen H, Lin X (2016) Experimental investigation of surface integrity in finish dry hard turning of hardened tool steel at different hardness levels. Int J Adv Manuf Technol 77(9–12):1655–1669
3. Tang L, Sun Y, Li B, Shen J, Men G (2019) Wear performance and mechanisms of PCBN tool in dry hard turning of AISI D2 hardened steel. Tribol Int 132:228–236
4. Soumikh R, Ramanuj K, Amlana P et al (2018) A Brief Review on Machining of Inconel 718. ICMPC_2018, Materials Today: Proceedings, 5:18664–18673
5. Sun S, Brandt M, Dargusch M (2010) Machining Ti-6Al-4 Valloy with cryogenic compressed air cooling. Int J Mach Tools Manuf 50:933–942
6. Yu N, He N, Li L (2010) Effect of refrigerated air cutting on tool wear in high-speed cutting of difficult-to-cut materials.Tribol, 30(5):487–490
7. Boswell B, Voges E (2011) The effect of combined cold air and minimum liquid cooling on end milling. Int Conference on Mech, Industrial, and Manuf Eng. Melbourne, Australia, (15–16):40–43
8. Liu N, Chiang K, Hung C (2013) Modeling and analyzing the effects of air-cooled turning on the machinability of Ti-6Al-4V titanium alloy using the cold air gun coolant system. Int J Adv Manuf Technol 67(5–8):1053–1066
9. Jozic S, Bajic D, Celent L (2015) Application of compressed cold air cooling: achieving multiple performance characteristics in end milling process. J Clean Prod 100:325–332
10. Kopac J, Pusavec F, Krolczyk G (2015) Cryogenic machining, surface integrity and machining performance. Archives of Mater Sci and Eng 71(2):83–93
11. Arruda ÉM, Brandão LC (2018) Performance study of multilayer carbide tool in high-speed turning of API 5L X70 pipeline steel using a cold air system. Int J Adv Manuf Technol 94(1–4):85–103
12. Anthony-Xavior M, Adithan M (2009) Determining the influenceof cutting fluids on tool wea rand surface roughness during turning of AISI 304 austenitic stainless steel. J Mater Process Technol 209:900–909
13. Saini A, Dhiman S, Sharma R, Setia S (2014) Experimental estimation and optimization of process parameters under minimum quantity lubrication and dry turning of AISI-4340 with different carbide inserts. J Mech Sci Technol 28(6):2307–2318

14. Pervaiz S, Deiab I, Rashid A, Nicolescu M (2017) Minimal quantity cooling lubrication in turning of Ti6Al4V: Influence on surface roughness, cutting force and tool wear. P I Mech Eng, Part B. J Eng Manuf 231(9):1542–1558
15. Masoudi S, Vafadar A, Hadad M, Jafariand F (2018) Experimental investigation into the effects of nozzle position, workpiece hardness, and tool type in MQL turning of AISI 1045 steel. Mater and Manuf Process 33(9):1011–1019
16. Makhesana MA, Baravaliya JA, Parmar RJ, • Mawandiya BK, Patel KM (2021) Machinability improvement and sustainability assessment during machining of AISI 4140 using vegetable oil–based MQL. J Braz Soc Mech Sci and Eng 43:535
17. Lin H, Wang C, Yuan Y, Chen Z, Wang Q, Xiong W (2015) Tool wear in Ti-6Al-4V alloy turning under oils on water cooling comparing with cryogenic air mixed with minimal quantity lubrication. Int J Adv Manuf Technol 81(1–4):87–101
18. Wang C, Lin H, Wang X, Zheng L, Xiong W (2017) Effect of different oil-on-water cooling conditions on tool wear in turning of compacted graphite cast iron. J Clear Prod 148:477–489
19. Yao K, Wang C, Ding F, Sui J, Li S (2021) Effect of nozzles on cutting performance when machining with oil-on-water cooling technique. J Adv Manuf Technol 112(1–2):313–322
20. Liu Z, Wan Y, Zhou J (2006) Tool materials for high speed machining and their fabrication technologies. Mater Mech Eng 5(30):1–4
21. Yallese MA, Chaoui K, Zeghib N, Boulanouar L, Rigal JF (2009) Hard machining of hardened bearing steel using cubic boron nitride tool. J Mater Process Technol 209(2):1092–1104
22. Bouchelaghem H, Yallese M, Mabrouki T, Amirat A, Rigal F (2010) Experimental investigation and preformance analysis of CBN insert in hard turing of cold work tool steel (D3). Mach Sci Technol 14(4):471–501
23. Ding Z (2016) Research on the machinability in high speed machining of powder metallurgy material. Dissertation, Hefei University of Technology
24. Anthony Xavior M, Manohar M, Jeyapandiarajan P (2017) Tool wear assessment during machining of inconel 718. Procedia Eng 174:1000–1008
25. Gupta MK, Mia M, Jamil M, Sigh R, Singla AK, Song Q, Liu Z, Khan AM, Azizur-Rahman M, Sarikaya M (2020) Machinability investigations of hardened steel with biodegradable oil-based MQL spray system. Int J Adv Manuf Technol 108(3):735–748

Tables

Tables 5 is available in the Supplementary Files section.

Figures

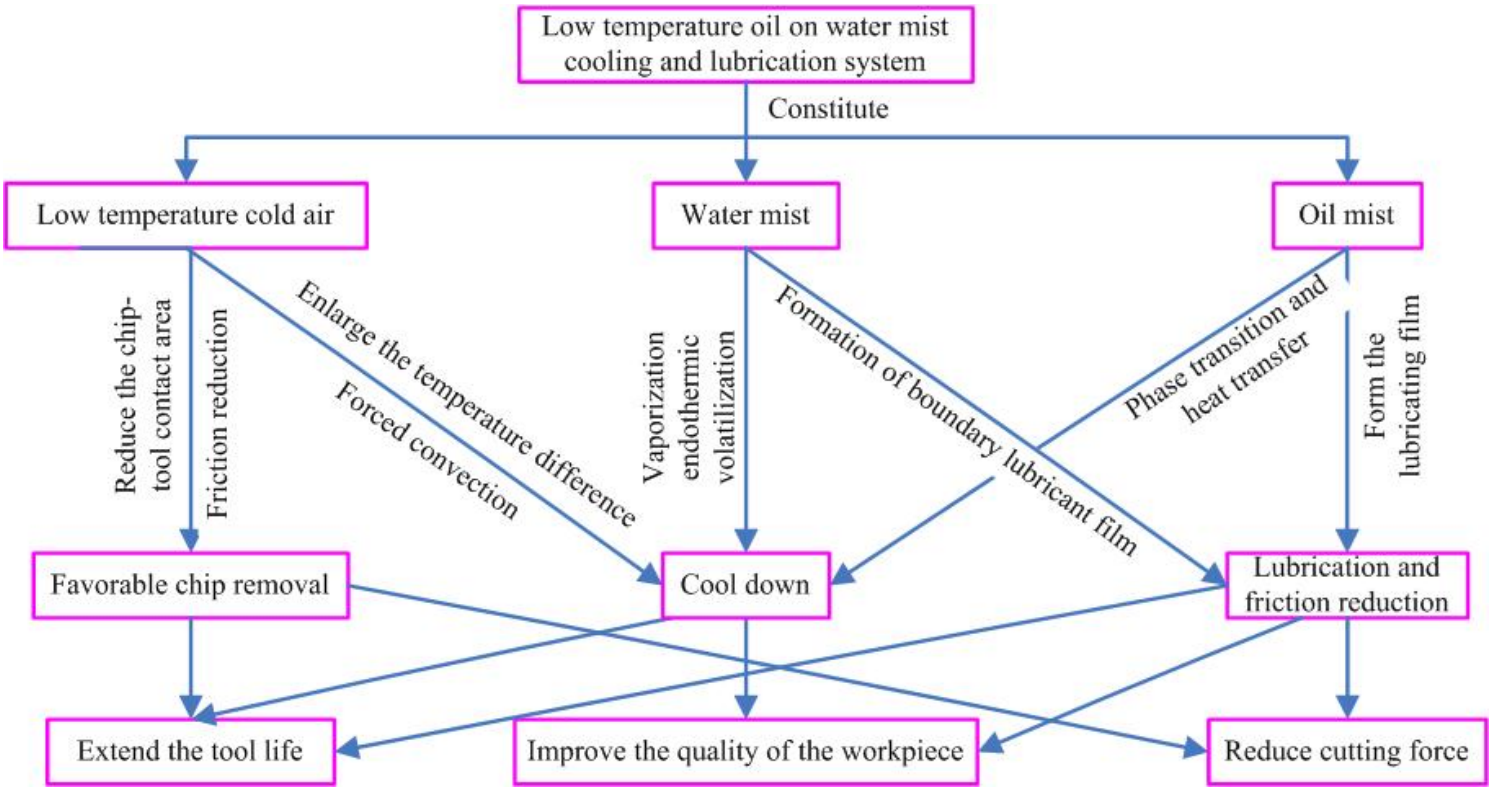

Figure 1

Cooling and lubricating mechanism model of LTOoW

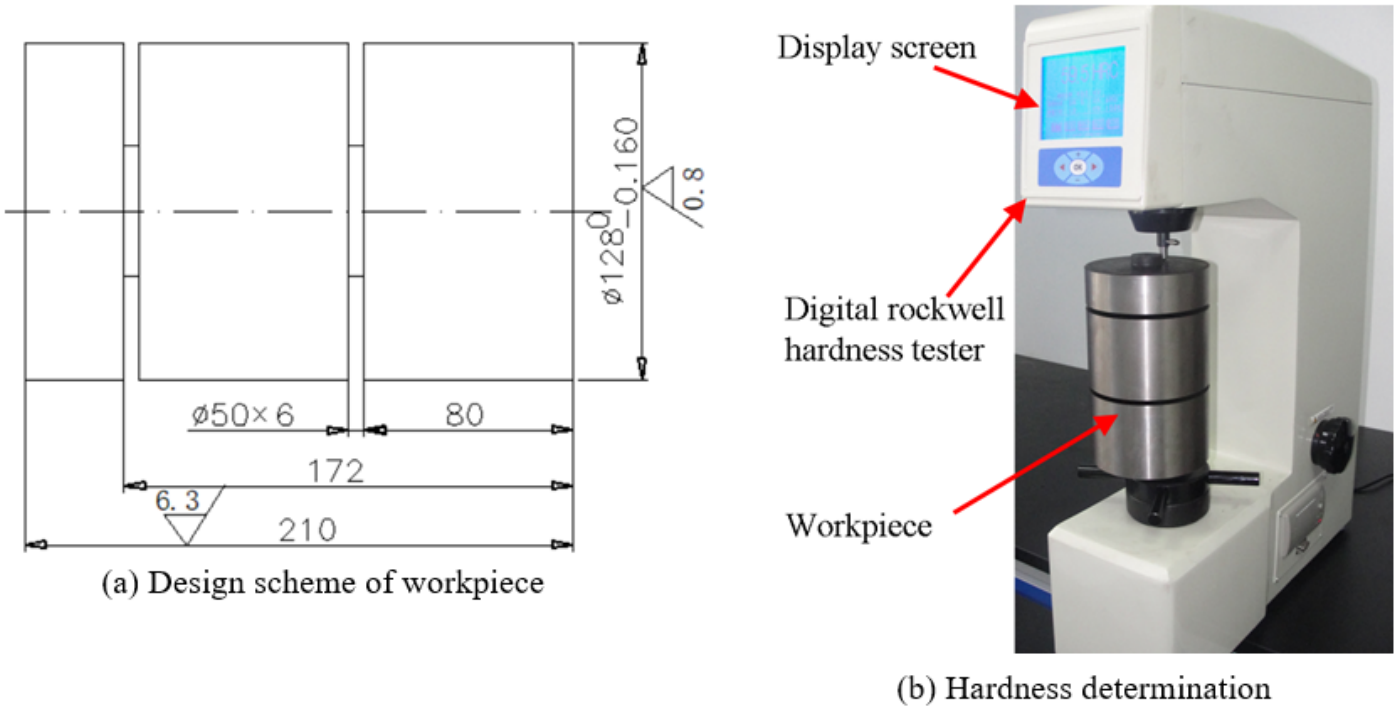

(a) Design scheme of workpiece

(b) Hardness determination

Figure 2

Design scheme and hardness determination

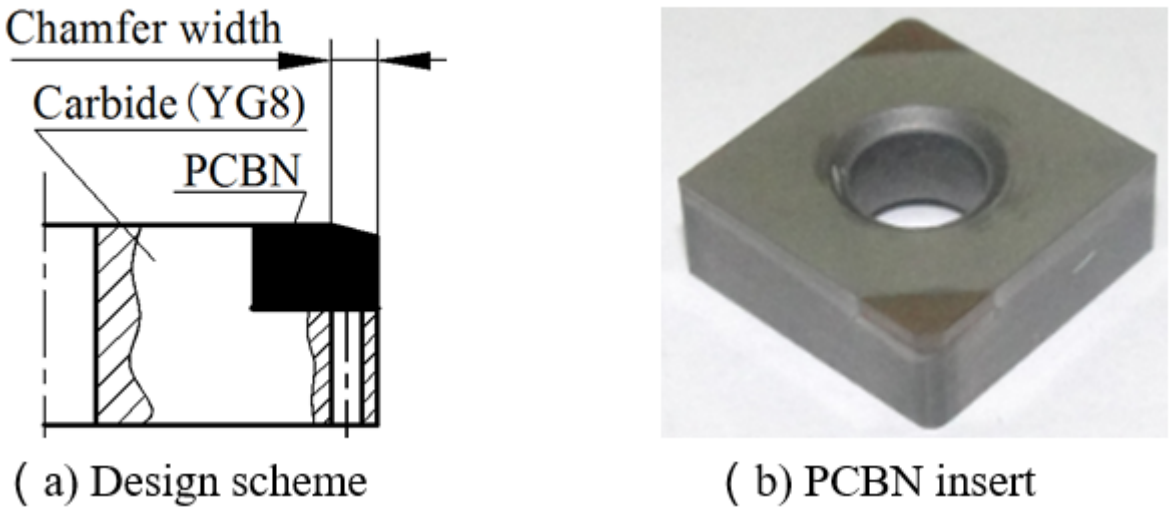

Figure 3

Composite PCBN insert utilized in this experiment

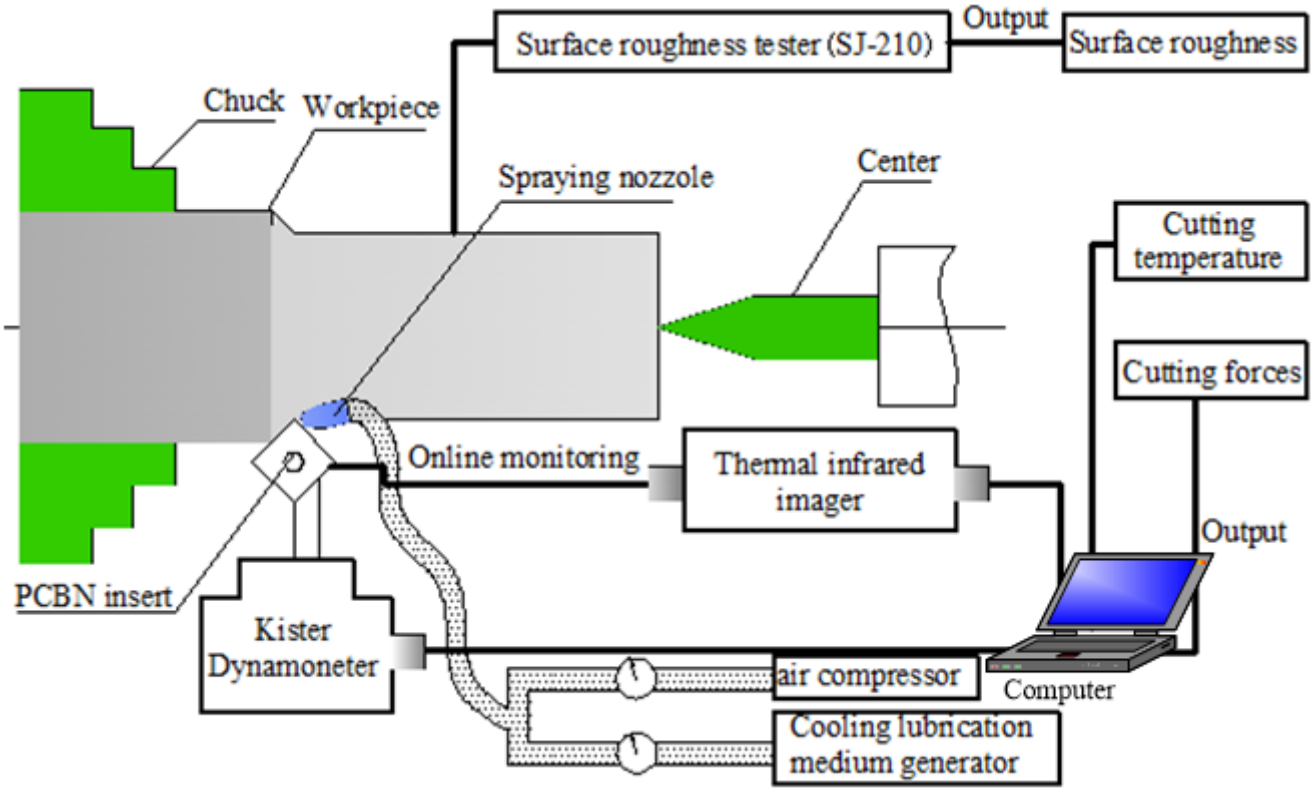

Figure 4

Schematic diagram of the turning experiment system

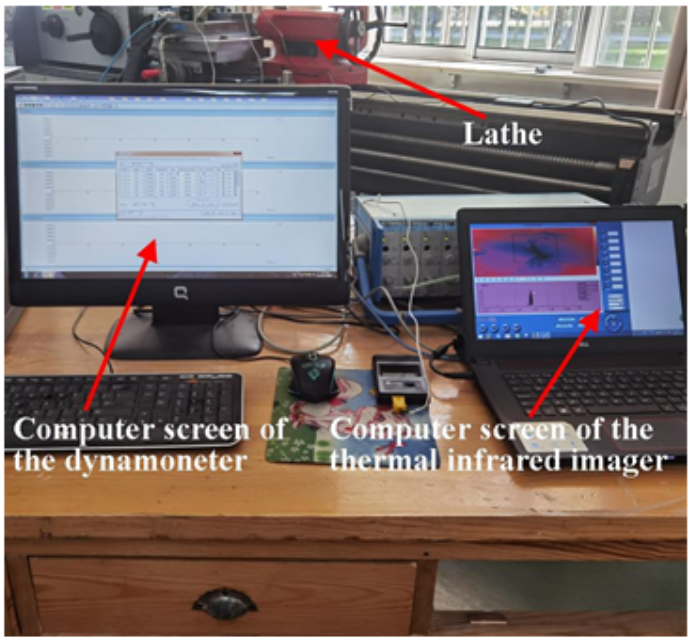

(a) Turning experimental setups

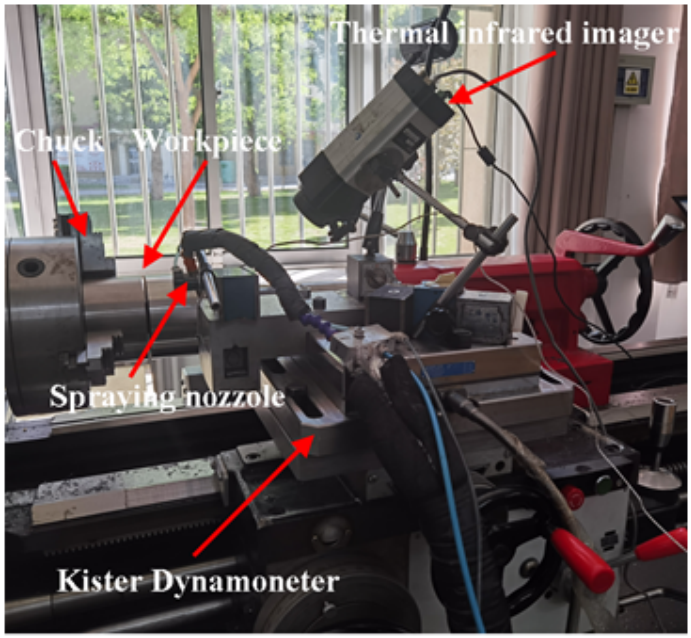

(b) Partial enlarged photograph

Figure 5

Turning experiment system

(a) Air compressor and air tank

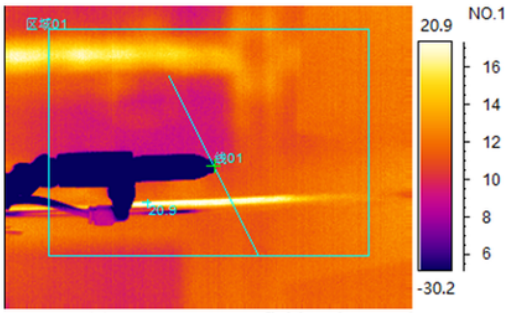

(c) Jet temperature field at the nozzle

(b) Low temperature compound spray cooling equipment

Figure 6

LTOoW mist cooling and lubrication system

Figure 7

Surface roughness tester

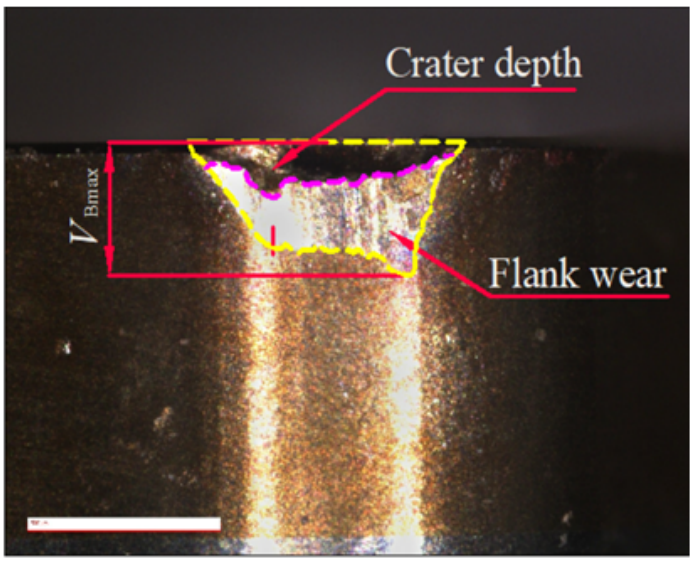

(a) Flank wear

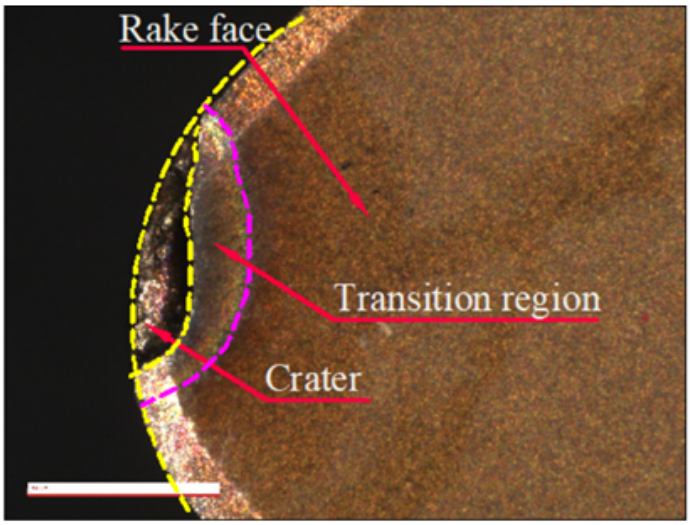

(b) Rake face wear

Figure 8

Tool wear measurement

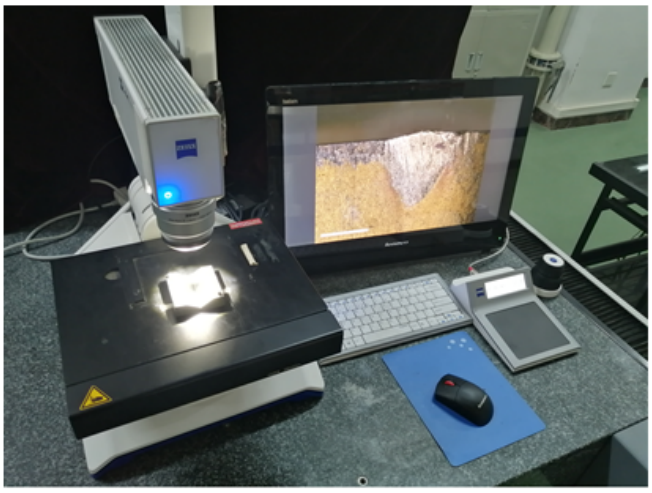

(a) Ultra depth of field microscope

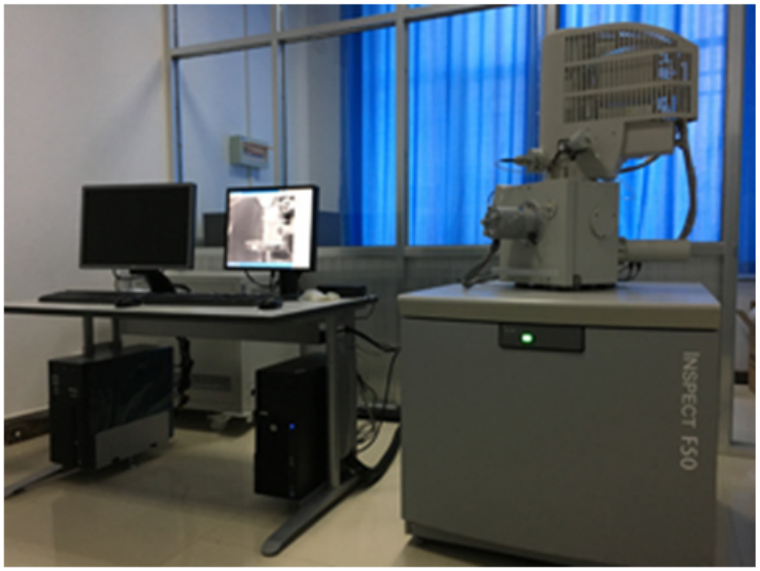

(b) Thermal field electron microscope

Figure 9

Instruments for measuring and analyzing tool wear

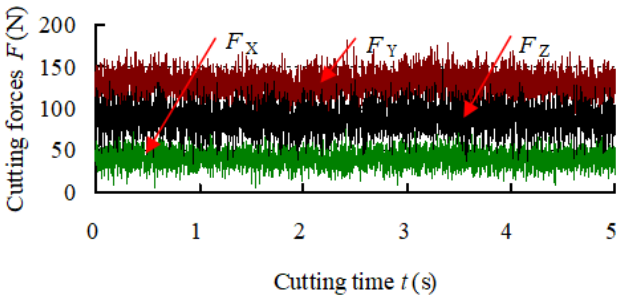

(a) The variation of the three-component cutting forces (v=140 m/min; f=0.15 mm/r; a_c=0.15 mm)

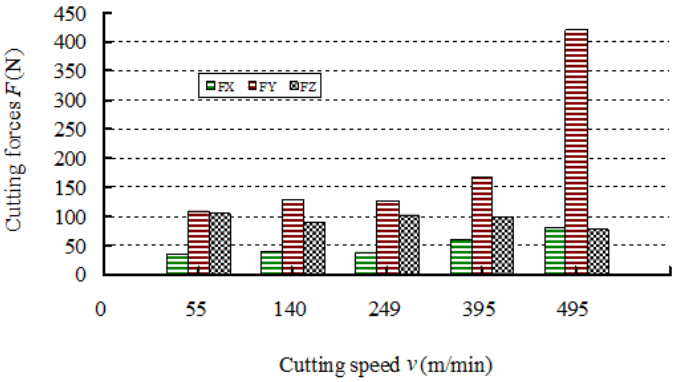

(b) The changing laws of the three-component cutting forces

Figure 10

The influence of the cutting speed on the three-component cutting forces

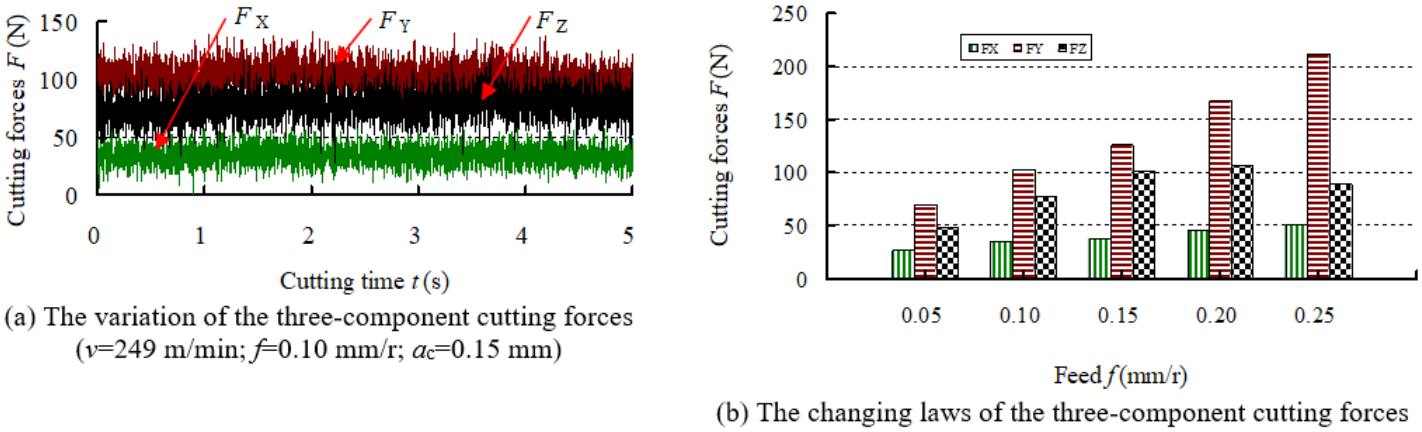

(a) The variation of the three-component cutting forces (v=249 m/min; f=0.10 mm/r; a_c=0.15 mm)

(b) The changing laws of the three-component cutting forces

Figure 11

The influence of the feed on the three-component cutting forces

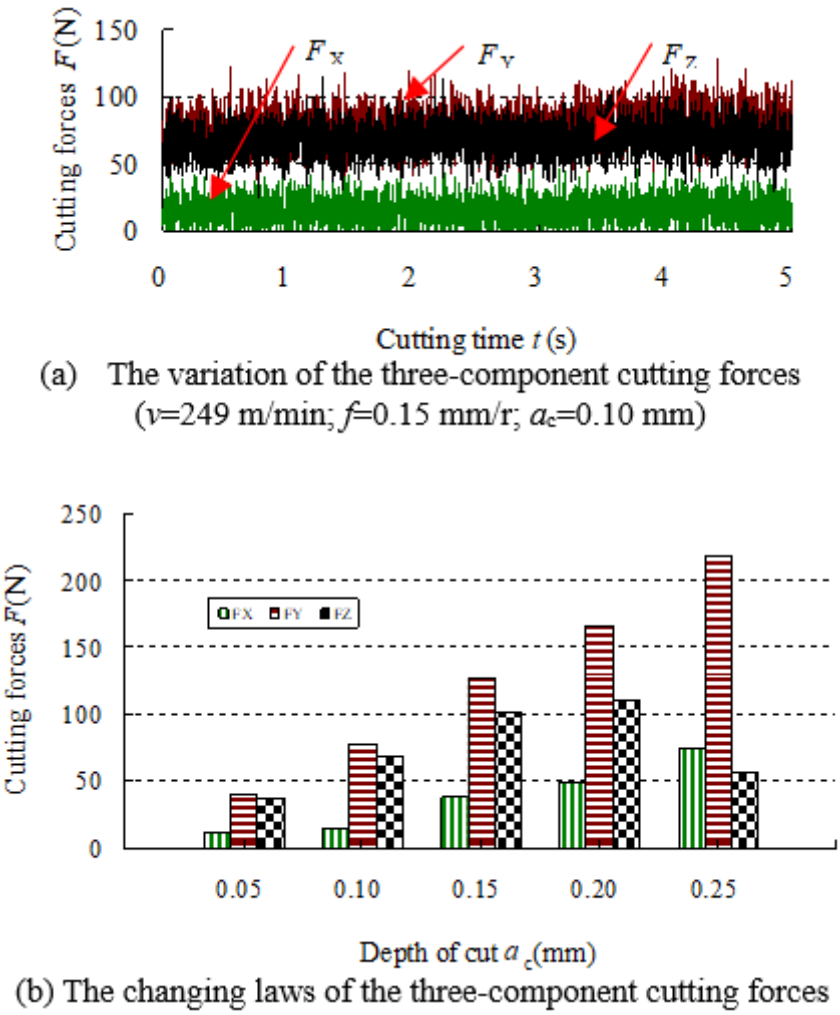

(a) The variation of the three-component cutting forces (v=249 m/min; f=0.15 mm/r; a_c=0.10 mm)

(b) The changing laws of the three-component cutting forces

Figure 12

The influence of the depth of cut on the three-component cutting forces

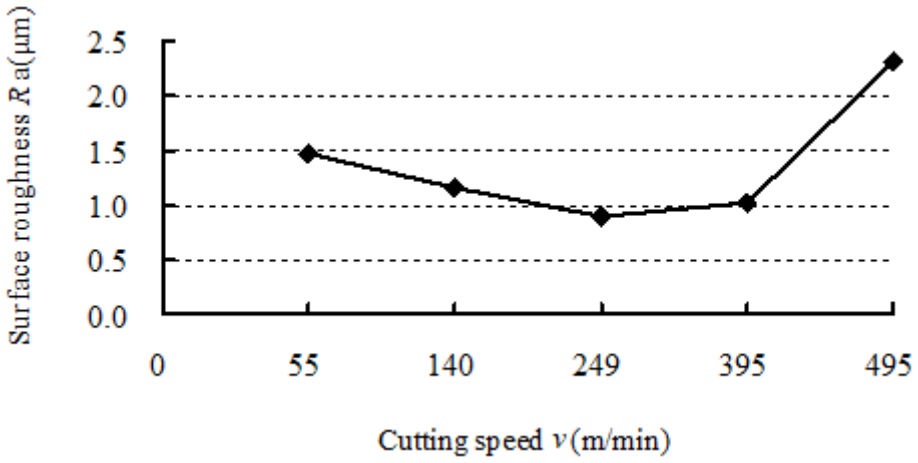

Figure 13

The influence of the cutting speed on surface roughness

(v=55-495 m/min; f=0.15 mm/r; a_c=0.15 mm)

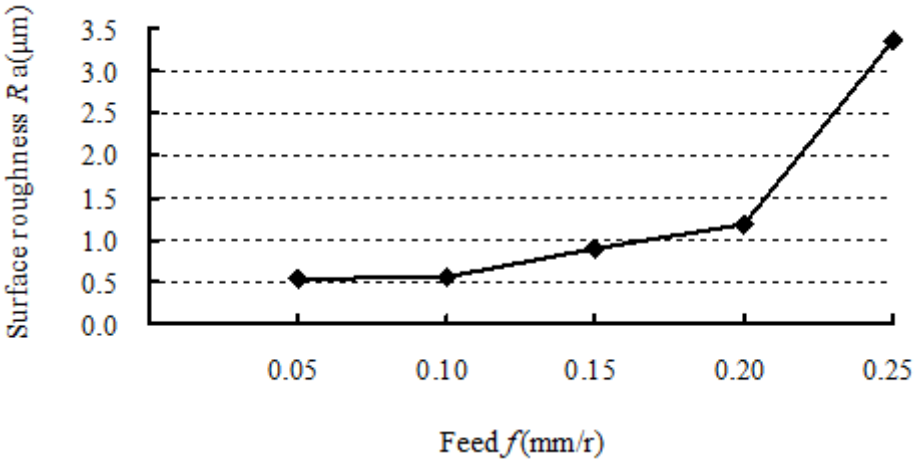

Figure 14

The influence of the feed on the surface roughness

(f=0.05-0.25 mm/r; v=249 m/min; a_c=0.15 mm)

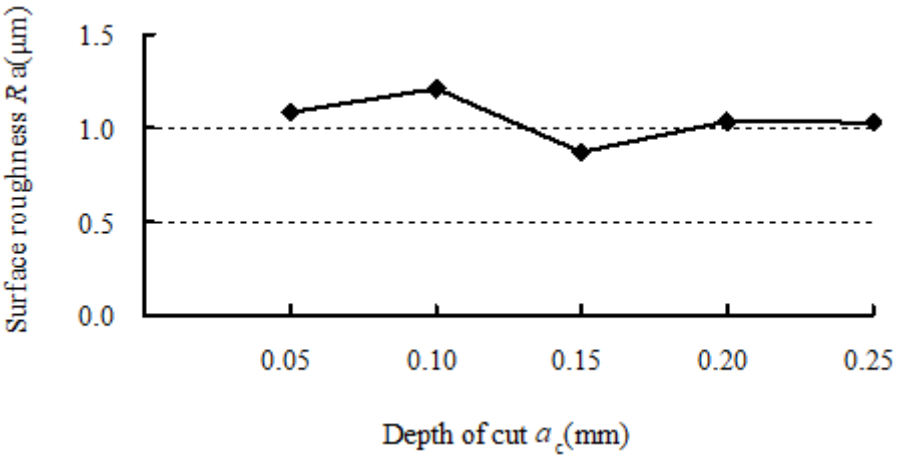

Figure 15

The influence of the depth of cut on the surface roughness

(a_c=0.05-0.25 mm; v=249 m/min; f=0.15 mm/r)

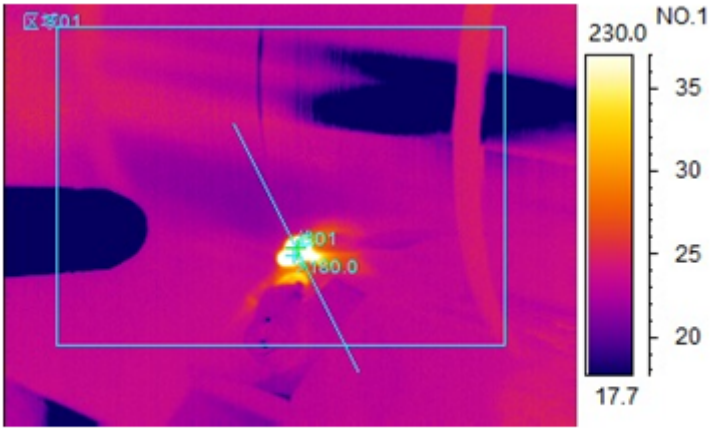

(a) The temperature field in a case of 55-m/min cutting speed

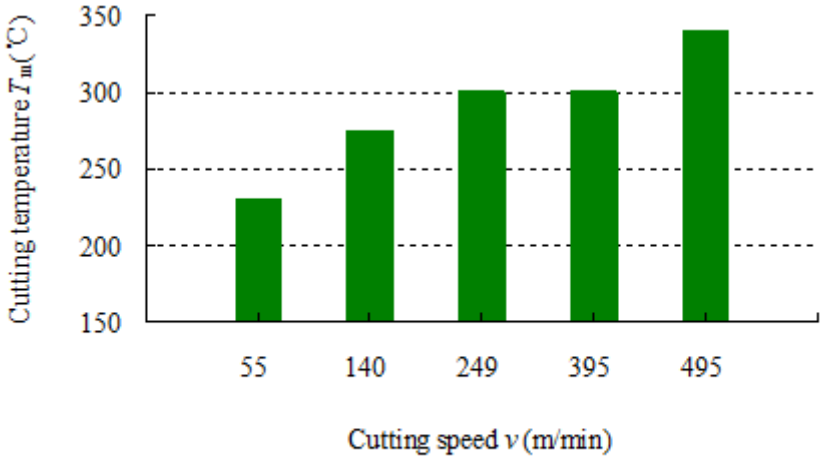

(b) Variation of the cutting temperature
(v=55-495 m/min; f=0.15 mm/r; a_c=0.15 mm)

Figure 16

Influence of the cutting speed on cutting temperature

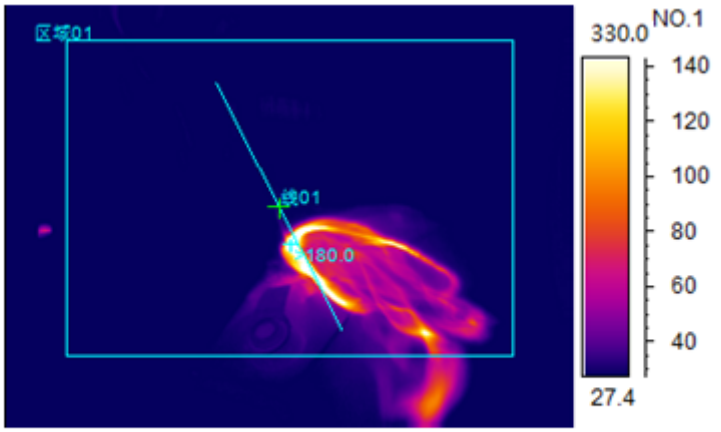

(a) The temperature field in a case of 0.05-mm/r feed

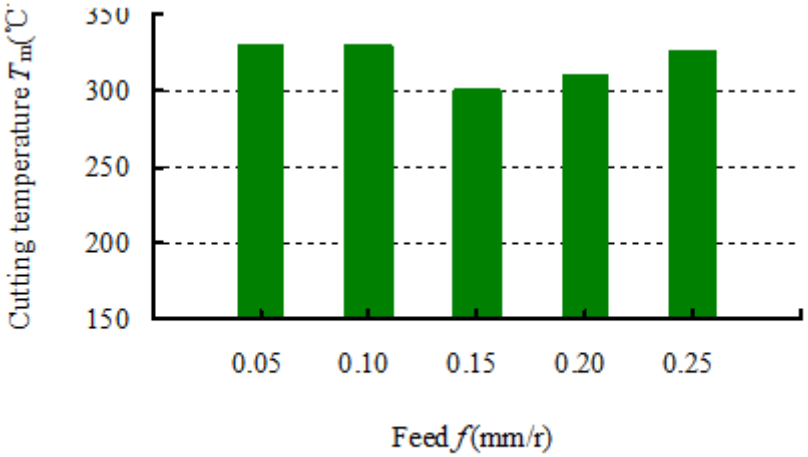

(b) Variation of the cutting temperature
(f=0.05-0.25 mm/r; v=249 m/min; a_e=0.15 mm)

Figure 17

Influence of the feed on cutting temperature

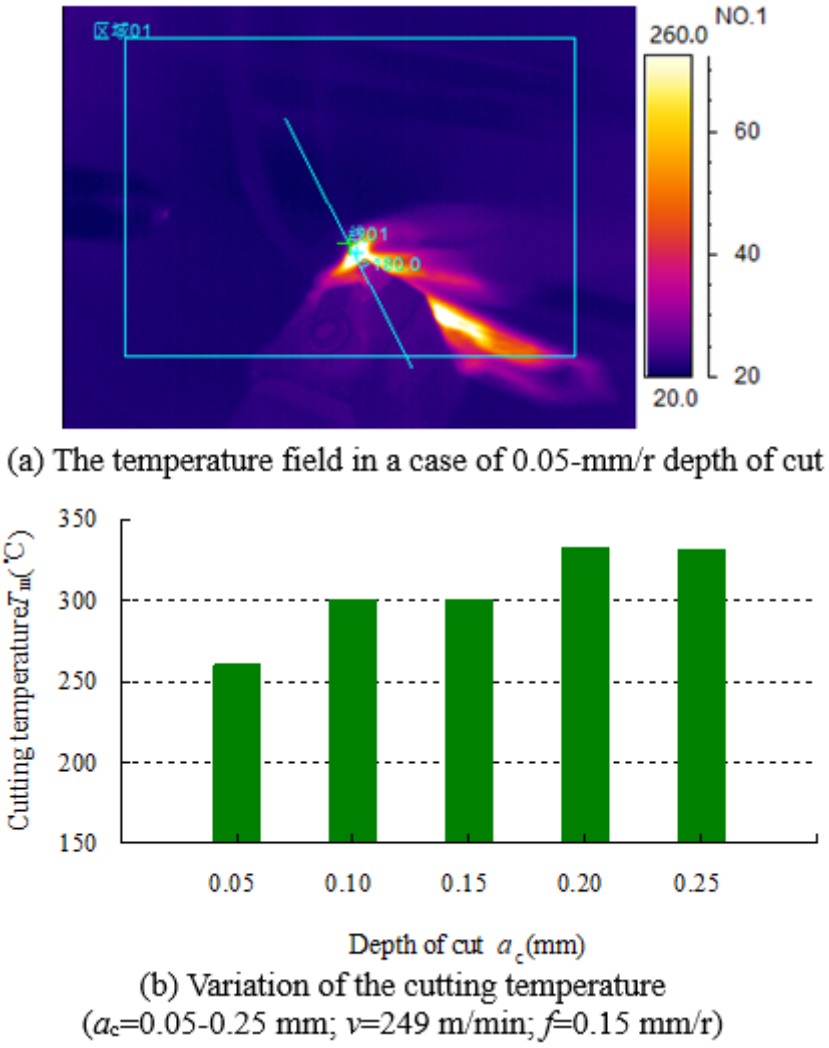

(a) The temperature field in a case of 0.05-mm/r depth of cut

(b) Variation of the cutting temperature (a_c=0.05-0.25 mm; v=249 m/min; f=0.15 mm/r)

Figure 18

Influence of the depth of cut on cutting temperature

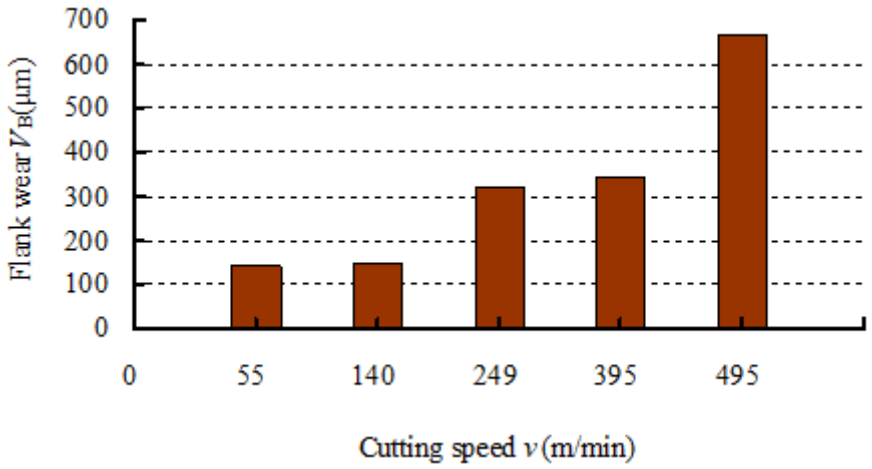

Figure 19

Influence of the cutting speed on the flank wear

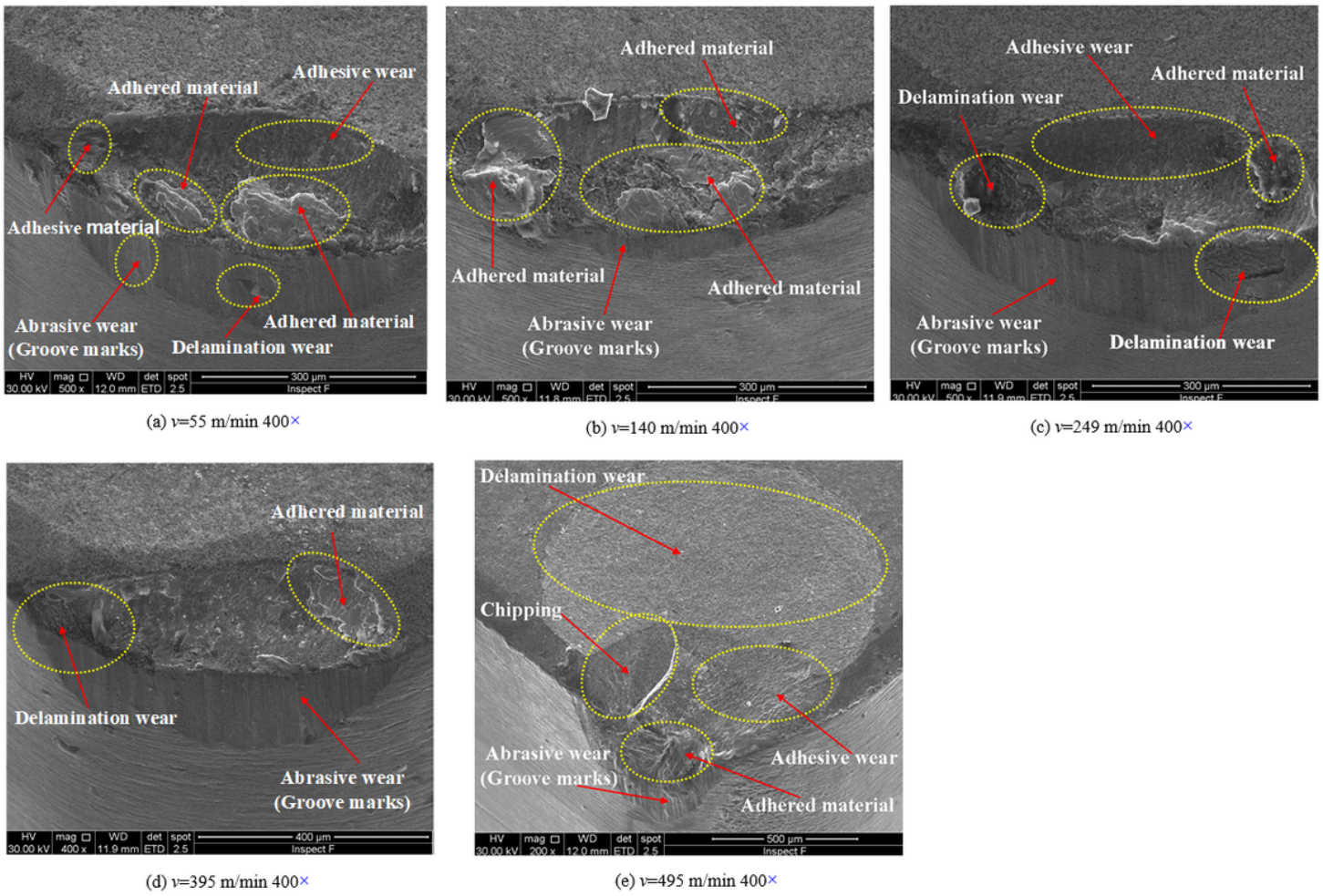

(a) v=55 m/min 400×

(b) v=140 m/min 400×

(c) v=249 m/min 400×

(d) v=395 m/min 400×

(e) v=495 m/min 400×

Figure 20

SEM micrographs of the worn tool at various cutting speeds

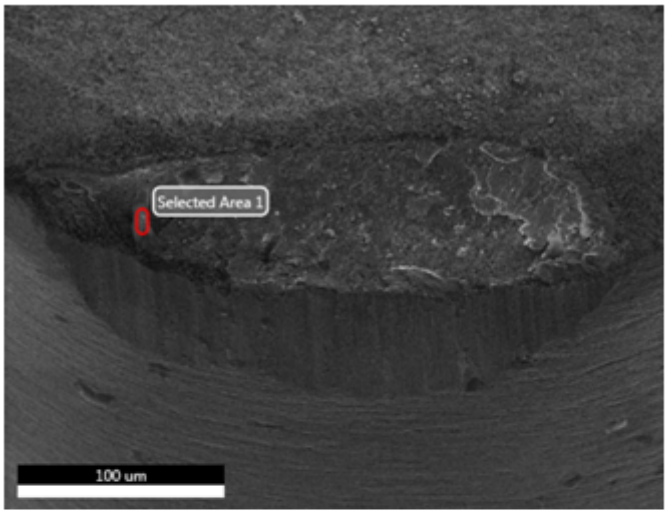

(a) Analysis zone

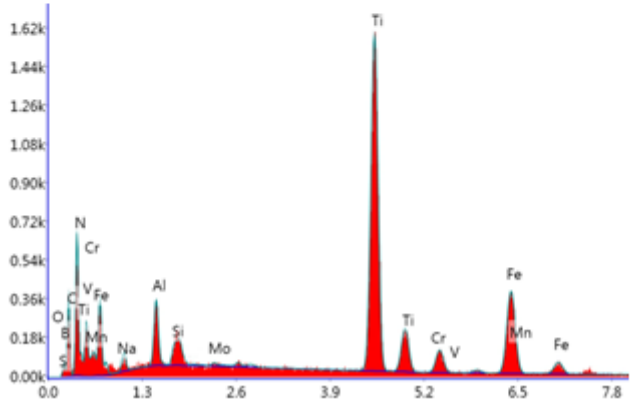

(b) EDS analysis

Figure 21

EDS analysis on crater wear zone at a 395 m/min

Supplementary Files

This is a list of supplementary files associated with this preprint. Click to download.

- Table5.docx